

UNDERSTANDING THE RELATIONSHIP BETWEEN MICROSTRUCTURE AND YIELD STRENGTH IN MEDIUM CARBON 54Si6Cr STEEL

^{1,2}Aleksandr GOKHMAN, ¹Zbyšek NOVÝ, ¹Pavel SALVETR, ¹Jakub KOTOUS

¹COMTES FHT a.s., Prumyslova 995, 334 41 Dobrany, Czech Republic, EU, <u>pavel.salvetr@comtesfht.cz</u>

² South Ukrainian National Pedagogical University (SUNPU), Staroprotfrankivska 26, 65020 Odessa,

Ukraine, alexander.gokhman@gmail.com

https://doi.org/10.37904/metal.2025.5126

Abstract

The contribution of microstructure elements to the yield strength of medium carbon 54SiCr6 steel was investigated. The microstructure was examined using scanning electron microscopy, transmission electron microscopy, electron back scattering diffraction and X-ray diffraction. The mechanical properties were assessed using a tensile test in accordance with CSN EN ISO 6892-1 standard. The influence of grain boundaries, dislocation density, size and volume fraction of carbide precipitates, distance between twins on the yield strength was estimated. The predominant contribution of twins to the yield strength for steel under investigation was established.

Keywords: Medium carbon steel, carbides, tempering, microstructure, twins, mechanical properties

1. INTRODUCTION

Actual material science of spring steels provides them with high strengthening and fatigue properties, but a low level of ductility. Important changes in mechanical properties should be attained through advanced thermomechanical processing supported by low addition of non-expensive alloying elements. In the search for high-performance, low-cost, highly reliable, and recyclable materials, quench-hardened martensitic steels are being used increasingly. At the same time, an improvement in their ductility is ensured by the addition of a tempering procedure. According to [1,2], the corresponding change in mechanical properties is determined mainly by the refinement of prior austenite grains (PAG) and PAG subunits (packets, blocks, and laths), leading to multi-level refinement of the hierarchical martensitic microstructure. The lath substructure, namely the structure of nanotwins, was observed in both low-carbon steels [3-6] and high-carbon steels [7], while there are no studies of twins in medium-carbon steels.

Therefore, the main goal of the present manuscript is to study nanotwins in medium-carbon spring steel 54SiCr6 after quenching and subsequent tempering. The development of the yield strength (YS), during quenching and tempering was determined. The microstructure was examined to reveal the evolution of microstructural features because of the processing used. The contribution of each microstructural element to the yield strength has been established. The effective grain size was found in the Petch–Hall relationship.

2. MATERIALS AND METHODS

The experimental material was medium carbon steel classified as 54SiCr6 (1.7102) steel. medium carbon steel B classified as 54SiCr6 (W.nr. 1.7102) according to ISO 8458-1 was investigated. The chemical composition is given in **Table 1**.



Table 1 Chemical compositions of the steel studied and 54SiCr6 steel, in wt%

Steel (in wt%)	С	Si	Cu	Mn	Cr	Ni	Мо	Fe
Experimental steel	0.56	1.54	1.48	0.70	0.77	0.056	0.016	Bal.
54SiCr6	0.51 – 0.59	1.2 – 1.6	_	0.5 – 0.8	0.5 - 0.8	-	-	Bal.

Experimental steel was prepared by vacuum induction melting in the COMTES FHT company and cast into a 45 kg ingot; the ingot was heated to 1050 °C and subsequently hot rolled to a 14 mm thick plate and air-cooled. The plates were normalized and annealed at 850 °C for 40 min. Cylindrical samples 13 mm in diameter and 120 mm in length were machined and subjected to various treatment regimes. First, all samples were heated to the same austenitization temperature of 900 °C for 20 min and oil quenched. Then, samples were tempered at temperatures of 250 °C, 350 °C, and 400 °C for two hours, followed by air cooling.

Yield strength was determined by tensile on samples after quenching and tempering at 250, 350, and 400 °C at room temperature. Three tensile specimens were tested for each heat treatment condition. The tensile specimens were 8 mm in diameter and 50 mm in length. Quasi-static tensile tests were performed according to CSN EN ISO 6892-1 at a rate of 0.75 mm/min.

Microstructural characterization was performed with a scanning electron microscope (SEM) JEOL IT 500 HR in the longitudinal direction of specimens. Metallographic samples were prepared by grinding and polishing, and the microstructure was revealed by etching with 3% Nital reagent. A transmission electron microscope (TEM) JEOL JEM 2200FS. Thin foils were prepared using the twinjet electropolishing method (Fishionne Electropolisher M220) in the solution of perchloric acid (5 mL) and methanol (95 mL) at -50 °C. Electron Back Scatter Diffraction (EBSD), Hikari Super camera, EDAX LLC, Mahwah, NJ, USA was used to determine crystallographic features such as grain boundaries and grain size. EBSD analysis was performed with a scanning step of 0.05 μ m on an area of 40×40 μ m. EBSD analysis provided an estimation of effective grain size (EGS). As in [8], the high-angle grain boundaries (HAGBs) with misorientation above 15° were used to determine EGS. These HAGBs were considered as arrest dislocation motion and were used in the Petch-Hall relationship.

X-ray Diffraction X-ray diffraction (XRD) analysis was carried out using BRUKER D8 DISCOVER diffractometer with Cu K α radiation (wavelength, λ = 0.15406 nm). Diffraction patterns were collected in the 2theta range from 30 to 120° with a step size of 0.02° and exposure time of 0.75 s/step. The retained austenite volume was characterized by the Rietveld refinement method using Topas software. The dislocation density, ρ , was determined by the modified Williamson–Hall (WH) method [9] from the full width at the half maximum (FWHM) and the diffraction angle of all peaks (101), (200), (211), (202), and (310).

The lattice friction stress σ_0 was estimated about 85 MPa [10]; solid solution strengthening $\Delta\sigma_{SS}$ was estimated for the given composition of steel 54SiCr6 about 155 MPa [10]. The grain boundaries strengthening $\Delta\sigma_g$ was estimated on the Petch-Hall relationship [11,12] – equation (1), where d is grain size, $k_y = 0.2$ MPa·m^{-1/2} [9]. The dislocation strengthening $\Delta\sigma_d$ was estimated on equation (2) [13], where ρ is dislocation density, M = 3 (Taylor factor), G = 76 GPa [9] (shear modulus), b =2.48 nm (Burger's vector). The carbide precipitate strengthening $\Delta\sigma_p$ was estimated on equation (3) [14], where V_f is volume fraction, and X represents the diameter of the precipitate. The twins strengthening $\Delta\sigma_t$ was estimated as difference of the experimental yield strength (YS_{exper.}) and calculated sum ($\sigma_0 + \Delta\sigma_{SS} + \Delta\sigma_g + \Delta\sigma_d + \Delta\sigma_p$).

$$\Delta \sigma_a = k_v \cdot d^{-1/2} \tag{1}$$

$$\Delta\sigma_d = \alpha M G b \sqrt{\rho} \tag{2}$$

$$\Delta\sigma_p = \left(\frac{0.538Gb\sqrt{V_f}}{X}\right) ln\left(\frac{X}{2b}\right) \tag{3}$$



3. RESULTS AND DISCUSSIONS

XRD analysis of the quenched steel 54SiCr6 detected diffraction peaks of martensite, cementite and retained austenite (RA) was detected about 8.2 %. This corresponds to a relatively low martensite start (Ms) temperature of 301.2 °C which was calculated using the equation (4) from [15].

$$M_S = 545 - 330C - 23Mn - 14Cr - 13Ni - 7Si + 2Al + 7Co - 5Mo - 13Cu (wt.\%)$$
(4)

By increasing the tempering temperature, RA decreased: RA = 7.5%, 5.4% and 1.1% for the tempering temperature of 250 °C, 350 °C, and 400 °C, respectively. It was revealed that the dislocation density also decreases monotonically with increasing tempering temperature $18.0 \cdot 10^{16} \, \text{m}^{-2}$, $14.0 \cdot 10^{16} \, \text{m}^{-2}$, $9.6 \cdot 10^{15} \, \text{m}^{-2}$, $8.4 \cdot 10^{15} \, \text{m}^{-2}$, respectively.

A representative TEM micrograph of tempering carbides in the interior of martensite laths are presented in **Figure 1**. The effective average radius (r), average distance (L) between transition carbides, and volume fraction (f) for the studied population of carbides (**Table 2**) are determined using NIS Elements 5.2 digital image processing and analysis software (Nikon, Tokyo, Japan), that provides the visualization of carbides and calculation their average area (S_{av}) . The value of r was found to be the radius of an effective sphere having the same area S_{av} . The value of L was found using the supplemented software developed by the authors. The value of L was calculated using equation (5) from [16], where L is the radius of the precipitate.

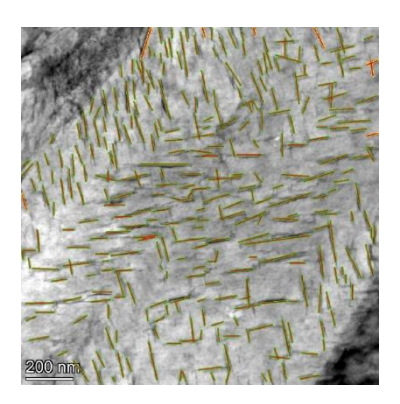


Figure 1 TEM study of carbides in BQT350

Table 2 The parameters of carbides population in steel 54SiCr6 after quenching and tempering

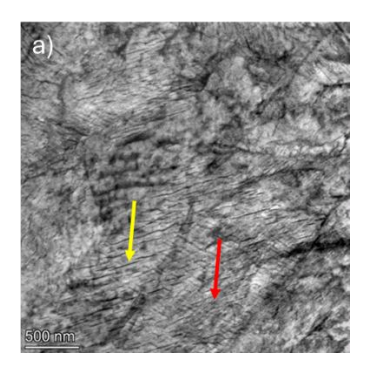
Sample	<i>r</i> (nm)	<i>L</i> (nm)	f (%)	
BQT250	18.1	100.8	3.9	
BQT350	15.3	86.8	3.9	
BQT400	14.0	97.2	3.0	

$$L = \sqrt{\frac{2}{3}} \left(\sqrt{\frac{\pi}{V_f}} - 2 \right) r \tag{5}$$

Representative TEM pictures of twins are presented in **Figure 2**. After quenching without tempering martensite laths with a width of 200–500 µm were observed. In numerous locations the formation of twins is visible. It is possible to distinguish two different types of twin populations – long and short twins. Long twins are usually visible in micrographs as long thin strips, not limited by martensite lath boundaries. The twinning plane is often parallel to the longitudinal axis of the martensite lath where twins are located. The population of long twins often covers several martensite laths with the same crystallography orientation and the same habit plane – martensite block. The short twin's population is usually limited to a single martensite lath. In this case, the twins run diagonally across the martensite lath. On one side they are limited by the lath boundary, while their second ends are located unevenly inside the martensitic lath. Sometimes short twins reach from one lath



boundary to the other, especially when the lath is smaller. The average distance between twins for the general population of long and short twins d_t was 13 nm. Already in the state after quenching without tempering, some contrast formations were organized into a system with predominant crystallographic planes. The origin of these formations remains an open question. However, most likely, the beginning of the precipitation of transition carbides was observed.



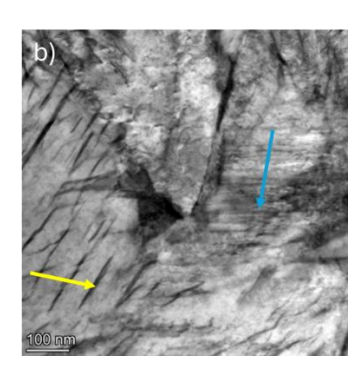


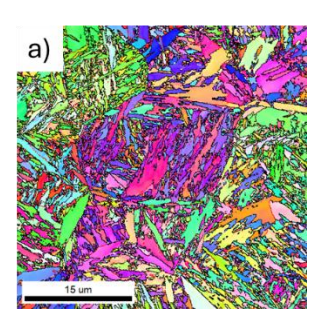
Figure 2 TEM BF micrographs of BQT 350 sample, a) the locality with transition carbides which replaced the original twinning population and b) neighbouring areas with remaining twins and with transition carbides. Yellow arrows show the transition carbides, blue arrows show the population of short twins. The red arrow designates the area with both transition carbides and rests of twins.

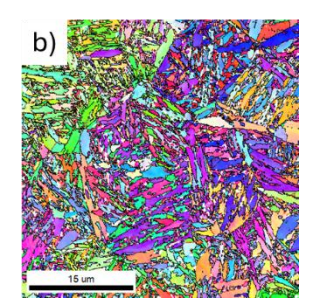
There are plenty of laths with transition carbides after quenching and tempering at 250 $^{\circ}$ C in most martensite laths. Sometimes these carbides have sharp straight morphology with a high degree of order. This arrangement is probably based on incipient precipitation visible even just after quenching. It is possible to observe twins also after tempering. Twins, initially present in the microstructure after quenching, change in their morphology during tempering (degenerated), and in some cases are also replaced by an expanding population of transition carbides. Thus, the number of both short and long twins decreased compared to the B0 state. The most typical changes in short twins are their shortening, widening, and sharpening of the ends located in the lath interior, the curvature of twinning planes, and increasing the spaces between the twinned bands. This space growth is probably due to the complete disappearance of some twin bands. Sometimes it is possible to trace a clear interaction of twins and the distribution of a population of transition carbides – precisely by long twins. Carbides growing in any case interrupt twins locally, in other cases, they completely replace the twin or even the entire part of the twin population. It is often possible to trace the carbides growth along the preliminary long twin. The value of d_t was 19 nm.

Transition carbides are the dominant substructure within martensite laths after tempering at 350 °C. Some populations of twins are completely replaced by transition carbides, others are significantly degenerated, while all populations are yet to show considerable morphology changes. Some populations of twins have been preserved, but they are overgrown with transition carbides. Transition carbides within a twin population exhibit lower ordering compared to carbides in a free matrix without twins. It can be appreciated that twins' degeneration seems to be more significant in short twins than in long twins. The total amount of twins is less compared to BQT250 state. The value of d_t was 21 nm. After quenching and subsequent tempering at a temperature of 400 °C for two hours, significant changes in the microstructure were observed. The number of transition carbides decreased, cementite particles appeared. Their appearance is clearly visible, for example, at the boundaries of the martensite plate, as well as inside it. The twin population sometimes probably retreated to transition carbides, both of which are later replaced by cementite particles. However, even after 400 °C tempering some twin populations can be observed. Also, this set of micrographs implies the hypothesis that the long twin population has a higher resistance to degeneration, while the short twin population exhibits a higher rate of decay. The value of d_t was 21 nm.



EBSD data for quenched state was found to be of poor quality due to a deformed lattice and numerous of dislocations. Therefore, the EBSD pattern for sample BQ0 was not used for analysis in our study. The EBSD orientation maps for BQT250, BQT350 and BQT400 are presented in **Figure 3**. The EGSs reached following values $0.36 \mu m$, $0.37 \mu m$ and $0.42 \mu m$, respectively.





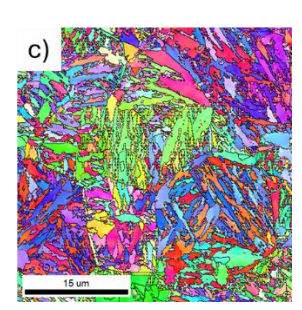


Figure 3 EBSD study of grain boundaries in BQT250 (a), BQT350 (b), and BQT400 (c).

In **Table 3**, there are listed the contribution of the lattice friction stress σ_0 , solid solution strengthening $\Delta\sigma_{SS}$, the grain boundaries strengthening $\Delta\sigma_g$, the dislocation strengthening $\Delta\sigma_d$, the carbide precipitate strengthening $\Delta\sigma_p$ and the twins strengthening $\Delta\sigma_t$ to the experimental yield strength YS_{exper}. Note that the relative contribution of twins to the yield strength is about 45 % and is dominant compared to the contribution of other features of the microstructure of the studied 54SiCr6 steel samples. The twins strengthening is almost the same for samples tempered at 250 °C and 350 °C but decreases significantly with increasing of tempering temperature to 400 °C. This is consistent with the observed effect of tempering on the average distance between twins d_t , which increased from 13 to 21 nm because of tempering. To describe the relationship between d_t , and $\Delta\sigma_t$, we apply the Petch–Hall relation (equation (5)), where $k_t = 1.1 \cdot 10^8$ MPa·m-1/2 was found for the studied samples of 54SiCr6 steel.

$$\Delta \sigma_t = k_t \cdot d^{-1/2} \tag{5}$$

Based on the predominant contribution of twins to the yield strength, it can be concluded that the d_t value can be considered as the EGS for 54SiCr6 steel, rather than as the size of the PAG, block, packet, or lath, as is commonly used as the EGS for steels with lower carbon content [1,2,17].

Table 3 Results of estimation of the contribution of each microstructural feature to the yield strength

Sample	σ₀ (MPa)	Δσ _{SS} (MPa)	Δσ _g (MPa)	Δσ _d (MPa)	Δσ _p (MPa)	Δσ _t (MPa)	YS _{exper} (MPa)
BQ0	85	186	190	-	-	-	1409
BQT250	85	186	167	333	241	843	1855
BQT350	85	186	139	329	271	848	1858
BQT400	85	186	130	309	246	670	1626

4. CONCLUSION

The effect of tempering on the contribution of grain boundaries strengthening, carbide precipitate strengthening and twins strengthening to the yield strength of 54SiCr6 steel was studied. It was found the predominant contribution of twins to the yield strength. Populations of short and long twins were found in quenched and subsequently tempered samples. The average distance between twins, d_t , increases with increasing tempering temperature. Relationship between the d_t and twins strengthening was described by the Petch-Hall relation with constant k_t is equal to $1.1 \cdot 10^8$ MPa·m^{-1/2}. The d_t value can be considered as the EGS for 54SiCr6 steel, rather than as the size of the PAG, block, packet, or lath, as is commonly used as the EGS for steels with lower carbon content.



ACKNOWLEDGEMENTS

This paper was created within the project National Centre of Competence ENGINEERING, No. TN02000018, which is co-financed from the state budget by the Technology agency of the Czech Republic under the National Centres of Competence Programme.

REFERENCES

- [1] GALINDO-NAVA, E.I., RIVERA-DÍAZ-DEL-CASTILLO, P.E.J. Understanding the factors controlling the hardness in martensitic steels. *Scripta Materialia*. 2016, Vol. 110, pp. 96-100.
- [2] SUN, C., FU, P., LIU, H., LIU, H.; DU, N., CAO, Y. The effect of lath martensite microstructures on the strength of medium-carbon low-alloy steel. *Crystals*. 2020, Vol. 10, p. 232.
- [3] PING, D.H., GUO S.Q., IMURA, M., LIU, X., OHMURA, T., OHNUMA, M., LU, X., ABE, T., ONODERA, H. Lath formation mechanisms and twinning as lath martensite substructures in an ultra low-carbon iron alloy. *Scientific reports*. 2018, Vol. 8, p. 14264.
- [4] PATTERSON, R. L., WAYMAN, C. M. Internal twinning in ferrous martensites. *Acta Metallurgica*. 1964, Vol. 12, pp. 1306–1311.
- [5] CHAKRABORTY, A., WEBSTER, R.F., PRIMIG, S. Lath martensite substructure evolution in low carbon microalloyed steels. *Journal of Materials Science*. 2022, Vol. 57, pp. 10359–10378.
- [6] ZHANG, W., SHANG, X., CHEN, X., CHEN, S., Liu, Z., Zhang, L. Quenching and Tempering-Dependent evolution on the microstructure and mechanical performance based on a laser additively manufactured 12CrNi2 alloy steel. *Materials*. 2023, Vol. 16, p. 3443.
- [7] SONG, W., DROUVEN, C., GALINDO-NAVA, E. Carbon Redistribution in Martensite in High-C Steel: Atomic-Scale Characterization and Modelling. *Metals*. 2018, Vol. 8, p. 577.
- [8] KIM, B., BOUCARD, E., SOURMAIL, T., SAN MARTÍN, D., GEY, N., RIVERA-DÍAZ-DEL-CASTILLO, P.E.J. The influence of silicon in tempered martensite: Understanding the microstructure–properties relationship in 0.5–0.6wt.% C steels. *Acta Materialia*. 2014, Vol. 68, pp. 169–178.
- [9] UNGÁR, T., DRAGOMIR, I., RÉVÉSZ, Á., BORBÉLY, A. The contrast factors of dislocations in cubic crystals: The dislocation model of strain anisotropy in practice. Journal of Applied Crystallography. 1999, Vol. 32, pp. 992–1002.
- [10] KIM, B., BOUCARD, E., SOURMAIL, T., SAN MARTÍN, D., GEY, N., RIVERA-DÍAZ-DEL-CASTILLO, P.E.J. The influence of silicon in tempered martensite: Understanding the microstructure–properties relationship in 0.5–0.6wt.% C steels. *Acta Materialia*. 2014, Vol. 68, pp. 169–178.
- [11] SALVETR, P., GOKHMAN, A., SVOBODA, M., DONIK, C., PODSTRANSKÁ, I., KOTOUS, J., NOVÝ, Z. Effect of Cu Alloying on Mechanical Properties of Medium-C Steel after Long-Time Tempering at 500 °C. *Materials*. 2023, Vol. 16, p. 2390.
- [12] HALL, E. O. The deformation and ageing of mild steel: III discussion of results. *Proceedings of the Physical Society. Section B.* 1951, Vol. 64, pp. 747-753.
- [13] PETCH, N. J. The orientation relationships between cementite and [alpha]-iron. *Acta Crystallographica*. 1953, Vol. 6, p. 96.
- [14] HUANG, M., RIVERA-DÍAZ-DEL-CASTILLO, P. E. J., BOUAZIZ, O., van der ZWAAG, S. Modelling strength and ductility of ultrafine grained BCC and FCC alloys using irreversible thermodynamics. *Materials Science and Technology*. 2009, Vol. 25, pp. 833–839.
- [15] GLADMAN, T. Precipitation hardening in metals. *Materials Science and Technology*. 1999, Vol. 15, pp. 30–36.
- [16] ISHIDA, K. Calculation of the effect of alloying elements on the Ms temperature in steels. *Journal of Alloys Compounds*. 1995, Vol. 220, pp. 126–131.
- [17] KANO, S., YANG, H.L., SUZUE, R., MATSUKAWA, Y., SATOH, Y., SAKASEGAWA, H., TANIGAWA, H., ABE, H. Precipitation of carbides in F82H steels and its impact on mechanical strength. *Nuclear Materials and Energy*. 2016, Vol. 9, pp. 331-337.